A Novel Technique for Gas Hydrate Formation at Predetermined Hydrate Saturation Using Excess Gas Method

Randeep Ravesh[1], Ayaj Ahamad Ansari[1], Sabyasachi Mohapatra[1],
Malay K. Das[1], Malcolm Lall[2], A.K. Misra[2] and P. K. Panigrahi[1]
[1]Department of Mechanical Engineering, Indian Institute of Technology, Kanpur, India
[2]GHRTC, Oil and Natural Gas Corporation, Panvel, Navi Mumbai, India

ABSTRACT

A 25 litre autoclave has been developed for comprehensive investigation of methane hydrate formation and dissociation process. This reactor has capability to carry out pressure measurement, multipoint temperature measurements, ultrasonic measurement, dynamic gas recovery measurement and several different types of optical diagnostics studies. This autoclave facilitates design of gas recovery strategies from gas hydrate.

A novel technique for forming hydrates of predetermined hydrate saturation is implemented. This technique is based on excess gas method and multi step gas injection. A mathematical expression is developed to calculate the fraction of moles utilized in hydrate formation at different stages of the hydrate formation process. Hydrate saturation at various gas injection stages is used to estimate. Furthermore, hydrate is dissociated using depressurization method. Periodic variation of pressure oscillation is observed during dissociation process indicating gas accumulation and release. The gas hydrate formation and dissociation has been successfully related to temperature distribution inside the porous media.

INTRODUCTION

Gas hydrates are solid crystalline compounds in which hydrogen-bonded water molecules trap gas molecules (Demirbas, 2010). Humphrey Davy discovered gas hydrates in 1810, but it remained only a lab curiosity for decades (Davy, 1811). Gas hydrates gained significant interest in academia and industry in the 1930s due to the observation that gas hydrates block gas pipelines (Hammerschmidt et al., 1934). It led to considerable effort for developing technologies to inhibit gas hydrates formation (Anderson and Prausnitz, 1986; Samimi, 2012). The most significant break through for the utilization of gas hydrates was accomplished in 1964 with the discovery of gas hydrates in Siberian permafrost (Makogon, 1965). It is estimated that the global hydrate-bound methane is $1.82.1 \times 10^{16}$ m^3 which is twice the amount of carbon available in all known fossil fuels on earth (Kvenvolden, 1988).

Gas recovery from gas hydrates requires its destabilization. The three primary methods of gas recovery are (i) depressurization (ii) thermal stimulation and (iii) inhibitor injection. The depressurization technique is the method of lowering the pressure of gas hydrate reservoir below the hydrate equilibrium, which makes hydrate unstable, and it dissociates (Liu et al., 2012a). During depressurization, the free gas layer is released first, followed by mixed gas and finally pure gas is released from hydrate (Li et al., 2012). The thermal stimulation method involves dissociating hydrates by increasing the in situ temperature above the gas hydrate equilibrium point (Tang et al., 2006). Thermal stimulation can be achieved by injecting substances such as hot water (Liu et al., 2012b). Li et al., (2008) concluded that the rate of instantaneous hydrate dissociation increases with increase in the salinity by hot brine injection. However, when the salinity is higher than a certain degree, the rate of instantaneous hydrate dissociation no longer continues to increase. The advantage of this method is that the hydrate decomposition process can be controlled by regulating the amount and rate of heat injection (Liu

et al., 2012b). However, the energy required for thermal stimulation is a challenge to make it economically feasible. Inhibitor injection method includes injection of thermodynamic inhibitors (such as methanol, brine) in hydrate-bearing media to dissociate hydrates. Inhibitors alter the formation conditions of hydrate phase equilibrium, which makes the hydrate system unstable and the hydrate decomposes (Bishnoi and Dholabhai, 1993; Mohammadi et al., 2008). However, inhibitors are expensive and large scale implementation may pose a challenge.

Sample preparation forms a crucial part in above hydrate dissociation studies. Very few studies available with focus on sample preparation for gas hydrate. Availability of efficient hydrate formation technique is an important step for carrying out technology development exercise. The hydrate formation techniques can be broadly classified (i) as excess gas method (Tang et al., 2007), (ii) excess water method (Chong et al., 2018) and dissolved gas method (Spangenberg et al., 2015). The excess gas method involves the introduction of water in porous media followed by the gas injection at a required over pressure. Hydrate formation is restricted by the amount of water. Generally, hydrates grown with above method illustrate grain cementing behavior in porous media (Priest et al., 2009).This method leads to preferential growth of hydrate at grain contacts which proliferates sediment strength and seismic velocities at even lower hydrate saturation (Stoll, 1979, Priest et al., 2009). Cementing hydrates are generally found around the base of gas hydrate stability region with an underlying formation of high dissolved methane concentration (Spangenberg et al., 2015; Rong, 2017).

Excess water method involves the introduction of a fixed number of gas molecules to porous media followed by injection of water in excess (Priest et al., 2009). Hydrate formation is limited by the amount of gas injected. In this method, hydrates are not restricted to form at inter-granular contact in comparison to the excess gas method and form pore filling hydrates (Spangenberg et al., 2015; Rong, 2017). This method simulates pore filling and load bearing morphology of gas hydrate formation in geological media (Rong, 2017). However, hydrate formed in nature is closer to the hydrate samples prepared using dissolved gas approach (Haacke et al., 2007). Dissolved gas approach involves hydrate formation from dissolved gas. The dissolved gas method is difficult to implement in the laboratory as it takes a significant amount of resources including time (Spangenberg et al., 2005).

Wang et al., (2013) introduced a novel method of hydrate formation in porous media involving water injection at multi-steps to obtain the required hydrate saturation. Here, multi-step injection of water/gas means the injection of water/gas is carried out during hydrate formation at different time intervals. This method is used in various studies (Li et al., 2002; Li et al., 2012). Multi step gas and water injection become essential in a large scale reactor to facilitate reasonable hydrate saturation because a single injection will involve requirement of high pressure injection condition (Wang et al., 2013).

Tupsakhare et al., (2017) used multi-step gas injection method to form hydrate in a large-scale reactor. However, their method did not aim to achieve predetermined hydrate saturation. The present study demonstrates a multi-step gas injection technique for obtaining predetermined hydrate saturations. An expression has been derived for calculating the fraction of methane moles utilized during hydrate formation. Subsequently, dissociation study has been carried out using the depressurization method at 0.85 of the equilibrium pressure.

EXPERIMENTAL DETAILS

This section discusses the experimental setup and procedure for the formation and dissociation of methane hydrate. The data analysis procedure for gas injection calculations follows later.

Experimental Apparatus

Figure 1 shows the experimental set up for formation and dissociation of methane hydrate and the photograph of the experimental set up Methane gas (CH_4) of 99.9% purity was obtained from M/s. Sigma Gases and Services and deionized water has been from DI plant of Indian Institute of Technology Kanpur, India. Indian standard sand (Tamil Nadu Minerals Limited (TAMIN)) of grade III was used to prepare the porous media whose details are presented in Table 1. The particle size of the sand is

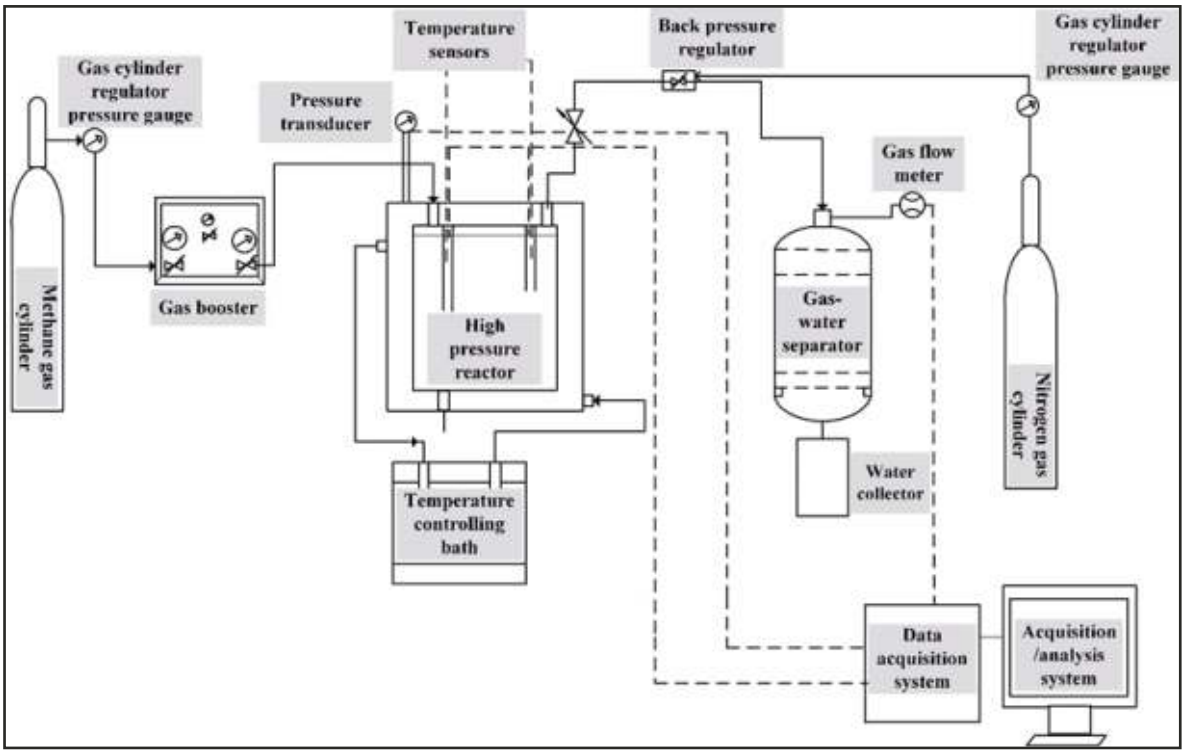

Fig. 1(a): Schematic diagram of the experimental setup.

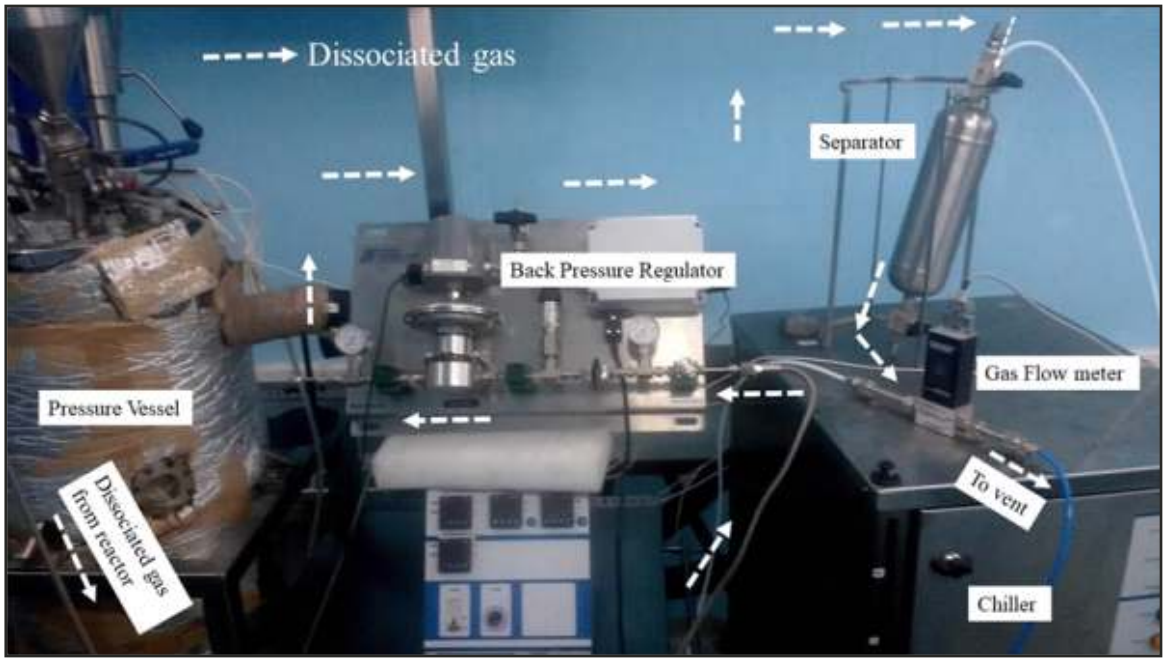

Fig. 1(b): Photograph of the experimental setup.

Table 1: Experimental details and material properties used in the work.

Parameters	Value	Source
Porous media particle size	0.09 - 0.5 mm	Tamil Nadu Minerals Limited
Porosity of porous media	0.38	Calculated using bulk density and particle density
Bulk Density of sand	1642.96 Kg/m^3	Experimentally calculated (Kisan et al., 1963)
Permeability	7.27 D	Kozeny - Carmen equation
Number of Gas Injection stages	3	Experimental operating condition
Water Injected	6 Kg	Experimental operating condition
Target Hydrate Saturation	0.24	Experimental operating condition
Actual Hydrate Saturation	0.2369	Experimental operating condition
Pore volume	8.59 L	Calculated
Molar density of hydrate (C_H)	7.35 moles/L	Chong et al., (2017)
Molar density of water (C_w)	55.5 moles/L	Chong et al.,(2017)
Reference temperature for solubility constant (t_0)	298.5 K	Sander (2015)
Henry's law solubility constant at T = 298.5 K	0.000014 (mol/m^3Pa)	Sander (2015)
Specific volume (V_g)	0.071428571 (m^3/Kg)	Wang et al., (2013)
Hydrate density (ρ_h)	912 Kg/m^3	Wang et al., (2013)
Molecular mass of methane hydrat (M_h)	124	Wang et al., (2013)
Critical temperature of Methane (T_h)	190.6 K	Reid et al., (1987)
Critical pressure of Methane (P_c)	4.599 MPa	Reid et al., (1987)
Acentric factor of Methane (ω)	0.012	Reid et al., (1987)

in the range of 0.09 mm-0.5 mm with the porosity and pore volume of the sand bed (V_{pore})equal to 0.38 and 8.59 L respectively. Figure 2 shows the SEM image of sand illustrating individual grains with irregular shapes. Gas received from methane cylinder was boosted using a booster pump to the desired injection pressure (55 bar) and supplied to the reactor chamber. The reaction chamber is made up of SS316 with an internal diameter of 232 mm and height of 622 mm. The capacity of the reactor is 25 L. Reactor was encased in a jacket of silicon oil (coolant liquid) to control the temperature of the reactor. For temperature measurement, the reactor is equipped with four resistance thermometers with an accuracy of ± 0.1°C: One pair of thermometer is located at height of 313 mm and the other pair located at the height of 326 mm. The radial distance of each pair of thermometers is 69 mm and 100 mm from the centre of the reactor respectively. Pressure transducer with an accuracy of ± 0.1 bar is placed at the top of the reactor head to record the pressure changes inside the reactor. Hydrate dissociation carried out by the depressurization method. The gas pressure was controlled by a backpressure regulator with a precision of ± 0.01 Bar. The separator placed after the back-pressure regulator is used to separate the water from the gas collected. The gas production is measured by a gas flow meter. Temperature and pressure recordings are acquired in a personal computer (PC) using the data acquisition system and a software.

Experimental Procedure

Initially, the reactor was cleaned with DI water and further purged by the nitrogen gas to clean any impurity. To maintain uniform mixing of water in sand, layers of required amount of sand and water ware added in 10 stages. Each stage uses 3.7 Kg sand and 0.6 Kg of water which finally results in water

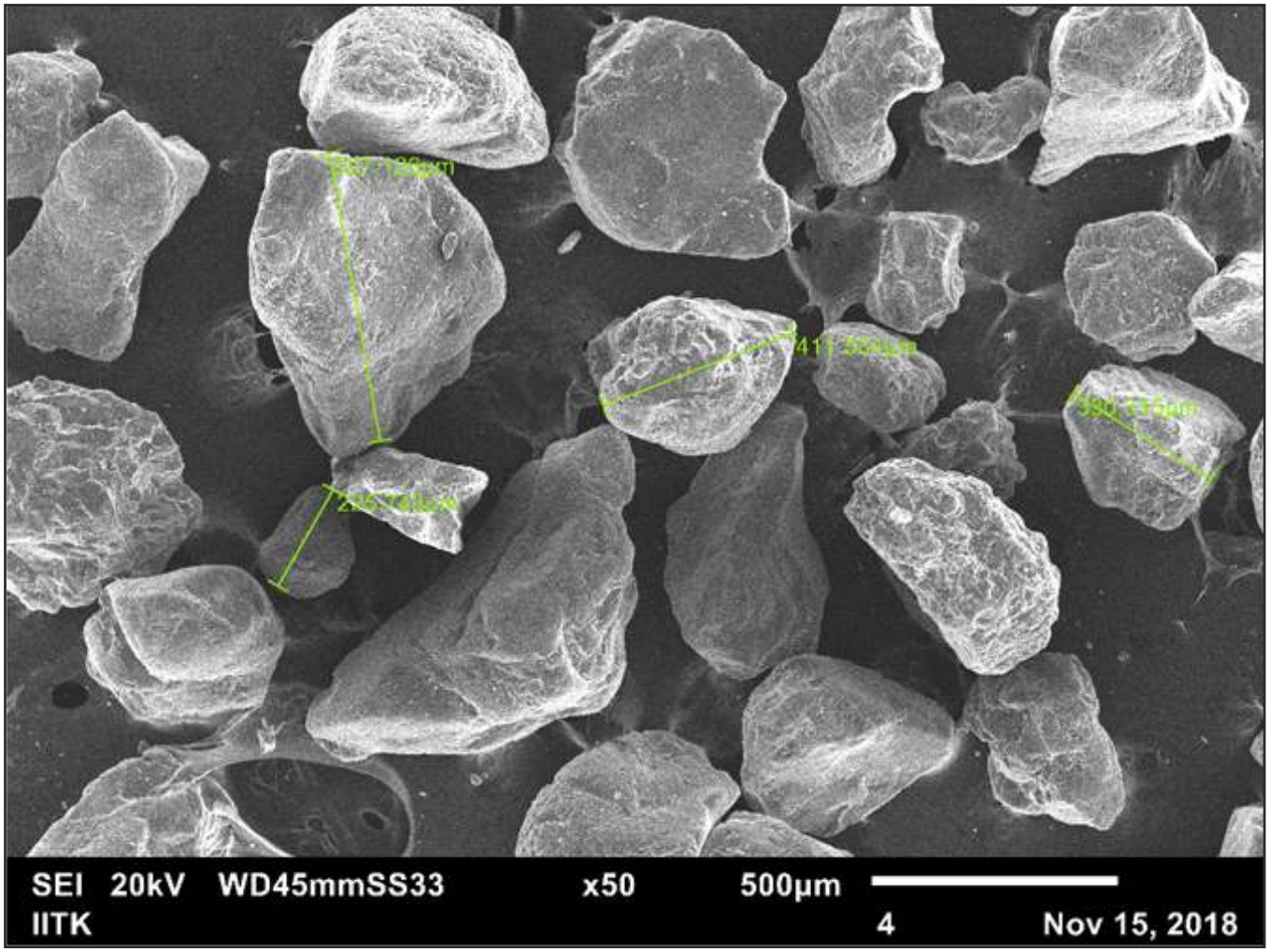

Fig. 2: SEM image of the sand sample illustrating irregular shape of sand particles.

saturation of 0.7 after all the sand layers are added. Chong et al., (2016) used similar method in preparing porous media for gas hydrate formation. The chamber is subsequently closed with the air-sealed head and evacuated till a vacuum pressure of 1KPa is achieved inside the chamber using a vacuum pump. The reactor subsequently connected to the gas supply line for gas injection and purging with Methane at 10 bar. Gas was injected subsequently to raise pressure to 55 bar in the first injection, and data acquisition is initiated to acquire pressure and temperature. The wall of the reactor was cooled to 2 °C using chiller. Hydrate formation inside the autoclave was indicated by an increase of temperature. The hydrate formation considered to be completed when there is no drop in pressure of the autoclave. Subsequently, gas is injected in two more additional stages.

Hydrate saturation reached to the desired value after three gas injection stages. A back pressure regulator was connected to the outlet of the reactor followed by gas-water separator and gas flow meter. The back pressure regulator set at 85% of the equilibrium pressure, and data acquisition is activated to acquire the gas dissociation condition. Dissociation of hydrate considered to be complete when the drop in pressure ceases for almost 5 hrs.

Gas Injection Calculations

The development of a procedure for obtaining predetermined hydrate saturation requires determination of required amount of gas and water moles, and calculation of saturation of hydrate at various gas injection stages. Procedure for determination of gas and water moles requirement is discussed below:

The chemical equation for methane hydrate formation can be represented as below, where N is the hydration number, which is equal to 6 for methane hydrates.

$$CH_4 +_+ NH_2O \rightarrow CH_4.NH_2O \quad (1)$$

It assumes that one mole of methane hydrate requires one mole of methane gas and six moles of water molecules. The number of moles of gas (n_{mt}) and water (n_w) required for formation of hydrate can be estimated using the following equations ((2) and (3)) respectively (Wang et al., 2013).

$$n_{mt} = V_{pore} S_h \rho_h / M_h + V_{pore} S_g / u_g + n_{m,a} \quad (2)$$

$$n_w = V_{pore} S_w \rho_w / M_W + N V_{pore} S_h \rho_h / M_h \quad (3)$$

Where, ρ_h is the density of hydrate formed, M_h is the molecular mass of hydrate, S_g is the gas saturation, $n_{m,a}$ is the moles of methane in the aqueous form, S_w is the water saturation, ρ_w is the water density, M_w is the molecular mass of hydrate.

Let us assume that n_m are the total moles of gas needed to be injected in the first injection stage. Considering the conservation of gas and water respectively for hydrate formation process, we can write;

$$n_{m,h} + n_{m,a} + n_{m,g} = n_m \quad (4)$$

$$n_{w,h} + n_{w,a} = n_w \quad (5)$$

Where, $n_{m,h}$ are the moles of methane in hydrate form, $n_{m,g}$ are the moles of methane in gaseous form, n_m are the moles of methane injected in the first injection, $n_{m,h}$ are the moles of water converted into hydrate form, $n_{w,a}$ are the moles of water present in the aqueous form, n_w are the moles of water required to achieve targeted hydrate saturation.

Let, f_t is the fraction of moles of methane utilized in hydrate formation to the total moles of gas injected, which can be written as;

$$n_h = n_{m,h} = f_t n_m \quad (6)$$

Where, n_h and $n_{m,h}$ are the moles of hydrate formed and moles of methane gas consumed for hydrate formation respectively. The fraction f_t is calculated by substituting $n_{m,h}$ from Eq. (6) in Eq. (4) and using state relation for $n_{m,g}$, resulting in;

$$f_t n_m + n_{m,a} + \left(\frac{PV_g}{ZRT} \right)_t = n_m \quad (7)$$

Where, P is the pressure of methane, Vg is the volume occupied by methane gas in the gaseous phase, Z is the compressibility factor, R is the gas constant, T is the temperature of methane. The volume occupied by methane gas in the gaseous phase (V_g) can be written considering the volumes occupied by water (V_w) and hydrate (V_h) as,

$$V_g = V_{pore} - V_w - V_h \quad (8)$$

Now, the volume occupied by hydrate and water can be expressed in terms of molar densities of water (C_w) and hydrate (C_h). Thus, we can write,

$$V_g = V_{pore} - \frac{n_{w,a}}{C_w} - \frac{n_h}{C_h} \quad (9)$$

Pitzer's correlation (Pitzer, 1955) is used to calculate the compressibility of the gas and using the gas critical temperature (T_c), pressure (P_c) and acentric factor (ω), compressibility factor (Z) is expressed as below:

$$Z_t = 1 + \left[0.083 - 0.422 \left(\frac{T_c}{T_t} \right)^{1.6} \right] \frac{PT_c}{P_c T_t} + \omega \left[0.139 - 0.172 \left(\frac{T_c}{T_t} \right)^{4.2} \right] \frac{PT_c}{P_c T_t} \quad (10)$$

Utilizing Eqs. (9) and (10) in Eq. (7), we have:

$$f_t n_m + n_{m,a} + \alpha_t \left(V_{pore} - \frac{n_{w,a}}{C_w} - \beta \right) = n_m \quad (11)$$

Where, $\alpha = \frac{P}{ZRT}$ & $\beta = \frac{n_h}{C_h}$ Substituting moles of water in aqueous state ($n_{w,a}$) from Eq. (5) in the above expression, we get:

$$f_t n_m + n_{m,a} + \alpha_t \left(V_{pore} - \frac{n_w - n_{w,h}}{C_w} - \beta \right) = n_m \quad (12)$$

Using Eq. (6) to account for the number of moles in hydrate form ($n_{w,h}$), we have,

$$f_t n_m + n_{m,a} + \alpha_t \left(V_{pore} - \frac{n_w - (f_t N n_m)}{C_w} - \beta \right) = n_m \quad (13)$$

Eq. (13) can be further manipulated to get the fraction of moles of methane converted to hydrate (f_t) and written as,

$$f_t = \frac{\alpha\left(V_{pore} - V_w\right) - \alpha_t\left(V_{pore} + \gamma\right) - n_{m,a}}{\alpha\left(V_{pore} - V_w\right) - \alpha_t\left(\frac{Nn_m}{C_w} - \frac{n_m}{C_h}\right)} \qquad (14)$$

Where, $\gamma = \frac{n_w}{C_w}$ Eq. (14) contains moles of methane dissolved in water ($n_{m,a}$) term, which can be calculated using the concentration of methane in the aqueous phase (C_a). Concentration, C_a can be calculated by using Henry's solubility constant (H) and partial pressure of that species in the gas phase under equilibrium conditions (P_t) as illustrated by Eq. (14) and using Henry's Law (Sander, 2015).

$$H = \frac{C_a}{p_t} \qquad (15)$$

Moreover, solubility constant values are available at reference temperature of 298.15 K (T_0)

$$H = H''\left(EXP\left(1900\left(\frac{1}{T} - \frac{1}{T_0}\right)\right)\right) \qquad (16)$$

and can be estimated at other temperature using Eq.(16) (Sander, 2015) as:

Where H'' is Henry's law solubility constant at temperature (T_0) = 298.5 K. Now, using T_0 = 298.15 K, H'' = 0.000014mol/m^3-Pa and T = 275.15 K, H at 275.15 K is equal to 2.38 X 10.$^{-5}$ mol/m^3-Pa. The concentration of methane in aqueous phase at p_t = 55 bar is equal to 0.13 moles/L, which is really small. Therefore, moles of methane gas dissolved in the aqueous phase is considerably less and may be neglected. Finally, Eq. (14) can be rewritten as:

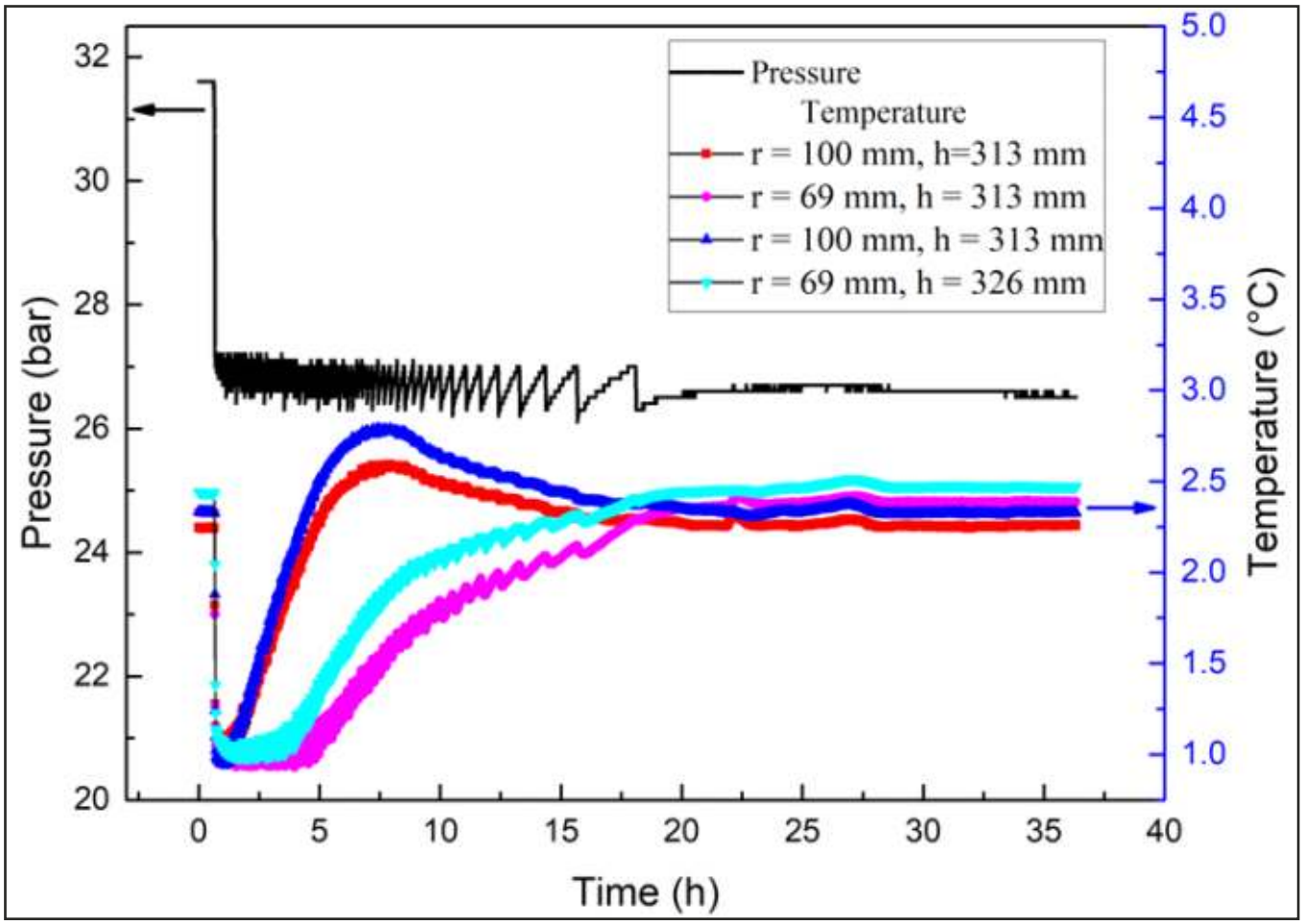

Fig. 3: Pressure and temperature evolution (at different radial (r) and axial locations (h)) during hydrate formation processes demonstrating three injection stages.

$$f_t = \frac{\alpha\left(V_{pore} - V_w\right) - \alpha_t\left(V_{pore} + \gamma\right)}{\alpha\left(V_{pore} - V_w\right) - \alpha_t\left(\frac{Nn_m}{C_w} - \frac{n_m}{C_h}\right)} \qquad (17)$$

Eq. (17) is the desired expression to calculate fraction of moles of methane converted to hydrate.

Hydrate saturation (S_h) can be easily calculated using f_t and expressed as;

$$S_h = \frac{V_h}{V_{pore}} = \frac{f_{t,i} n_m}{C_h V_{pore}} \qquad (18)$$

For subsequent injections, the generalized equation utilized for calculating the fraction of moles converted into hydrate at different injection stages is given as,

$$f_{t,i} = \frac{\alpha_i\left(V_{pore} - V_w\right) - \alpha_t\left(V_{pore} + \gamma\right)}{\alpha_i\left(V_{pore} - V_w\right) - \alpha_t\left(\frac{Nn_m}{C_w} - \frac{n_m}{C_h}\right)} \qquad (19)$$

Where "*i*" denotes the injection stage number. The values of parameters used to calculate Eq. (17) are summarized in the Table 1.

RESULTS AND DISCUSSION

The results from the present study have been discussed in two parts, i.e. gas hydrate formation and gas hydrate dissociation.

Gas Hydrate Formation

Figure 3 shows evolution of pressure and temperature during hydrate formation. After the first injection, pressure stabilizes around 54 Bar. The equilibrium temperature is 7.5°C at 54 Bar and reactor temperature is 3°C. The rapid drop in pressure and increase in temperature occurs due to initiation of nucleation and formation of hydrate. The subsequent drop in temperature is attributed to the cooling by the jacket. Subsequently, intermittent temperature peaks are observed, which was attributed to the transport of heat due to hydrate formation at neighbouring locations in porous media. These temperature spikes can also occur due to secondary hydrate formation. Breaking of hydrate layer can also lead to further hydrate formation due to enhanced diffusion of gas through the hydrate layer. Hydrate formation ceases at around 50 h. Temperature variation is observed in the radial direction during hydrate formation. The temperature away from the wall shows a higher increase in temperature in comparison to the region close to the wall because of the cooling at the wall. This indicates the importance of thermal transport with in hydrate-bearing porous media. Gas is subsequently injected in the second stage which causes pressure to increase from 32 to 55 Bar and temperature also increases from about 2.4°C to 3°C. In the second injection stage, hydrate formation takes plave at a slower rate due to reduction in pore permeability which causes gas to diffuse slowly. Formation of hydrate takes place for around 200 h which is 300% higher than pervious stage and final equilibrium temperature reached at 32 Bar. The third stage of formation process takes less time as fewer moles of gas are injected due to lower void volume because of the prior hydrate formation.

Hydrate saturation variation with time calculated using equation 15 is illustrated in figure 4. Parameters used for calculating hydrate saturation has been presented in table 1. The difference between equilibrium pressure and reactor pressure acts as a driving force for hydrate formation. Initially, hydrate saturation increases rapidly but slows down as pressure decreases towards equilibrium value due to decreased driving force. However, hydrate saturation increases with subsequent gas injection and continues to increase till the the onset of reduction in driving force. Hydrate saturation trend is similar to the nature of pressure profile during hydrate formation as pressure is the most crucial parameter influencing hydrate formation. Interestingly, hydrate saturation shows slow decrease during the second and third injections. This is because gas injection leads to small increase in temperature which dissociates hydrate to a small amount. The target saturation of the experiment and actual hydrate saturation are equal to 0.24 and 0.237 respectively. This shows the effectiveness of the technique and Eq. (17).

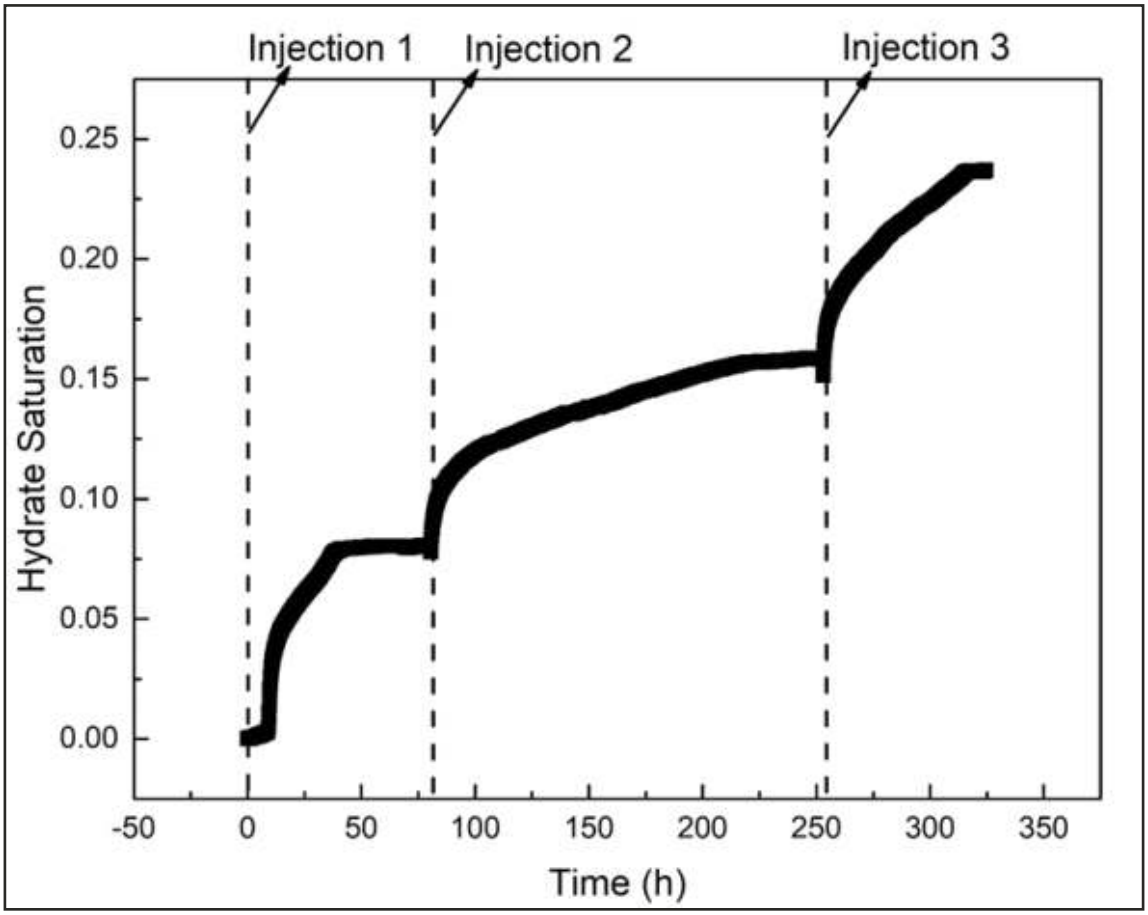

Fig. 4: Evolution of hydrate saturation with time during the formation process.

Figure 5 shows experimental conditions comparison with equilibrium curve obtained using Colorado School of Mines (CSMHYD during the entire experiment duration. Figure 5(a) shows initial cooling step (1-2) and subsequent hydrate formation step (2-3). However, the initial cooling of porous media is not included in figure 3. Initial cooling of porous media ensures conditions for hydrate formation enters in hydrate stability zone. Hydrate formation is marked by a rapid decline in pressure and a slight increase in temperature. Figure 5(b) depicts the second gas injection and hydrate formation. The second gas injection causes both pressure and temperature to rise (3-4), and subsequent hydrate formation causes pressure to fall again (4-5). Similarly, fig. 5(c) shows third gas injection stage (5-6) and hydrate formation stage (6-7). Hydrate dissociation stage (7-9) is illustrated in figure 5(d) using depressurization at a constant pressure of 2.7 MPa. Hydrate dissociation consists of two steps during depressurization. The first step includes rapid depressurization from reactor pressure to production pressure (7-8) and depressurization at constant production pressure (8-9). The hydrate dissociation stage is discussed in detail in the subsequent section.

Gas Hydrate Dissociation

Figure 6 shows the variation of temperature and pressure during hydrate dissociation using depressurization. For hydrate dissociation, the back pressure regulator is set at 2.7 MPa which is 85% of the equilibrium pressure at 2°C. Free gas release followed by mixed gas, and finally, gas comes out from hydrate dissociation. The pressure inside the reactor shows a periodic variation during hydrate dissociation. As hydrate dissociates, the back pressure regulator valve opens to release excess pressure, which subsequently gets closed due to the termination of the dissociation process. This is attributed to the periodic variation inside the reactor.

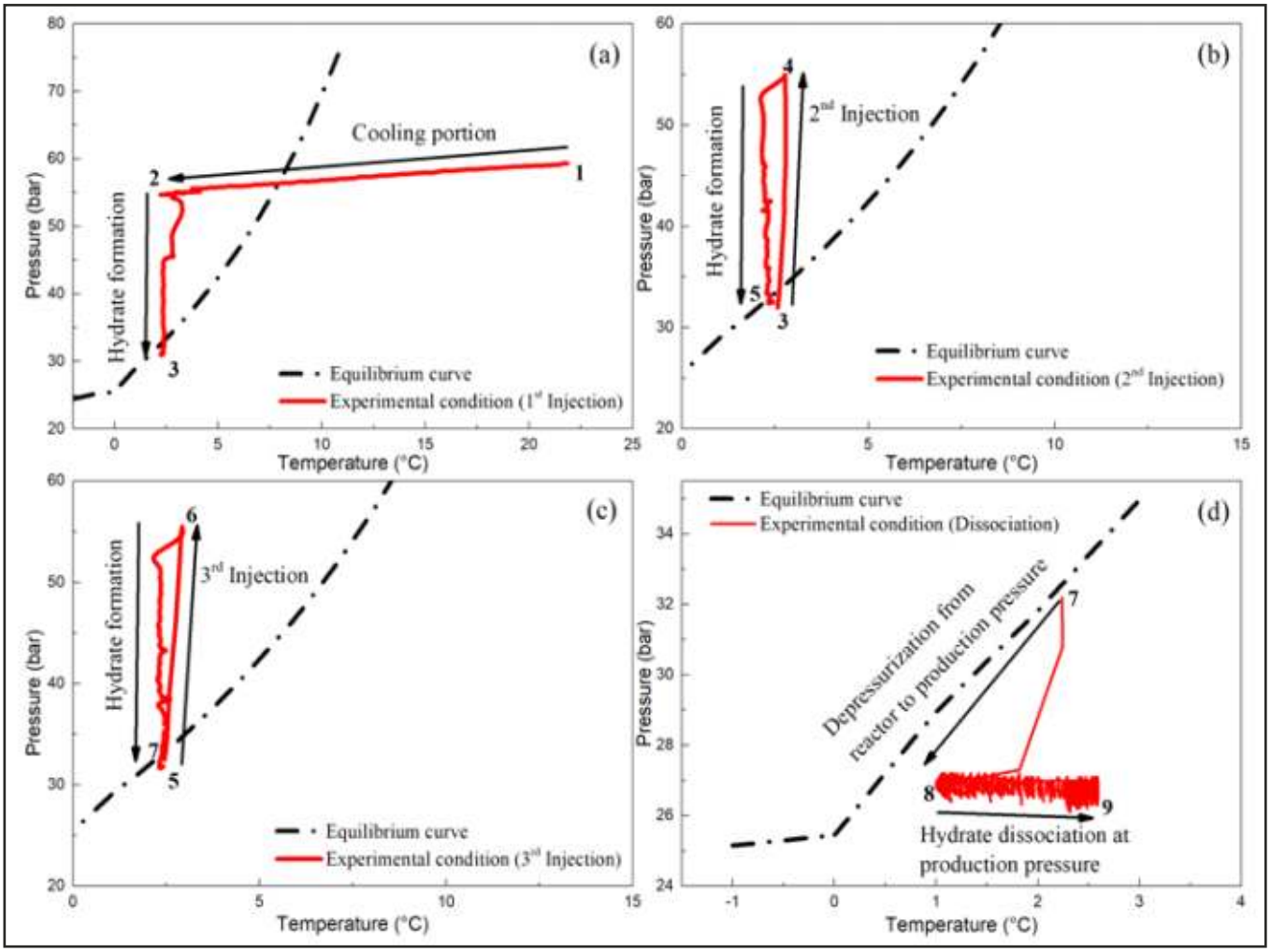

Fig. 5: Pressure-Temperature condition during different stages with reference to the equilibrium curve: (a) Initial cooling (1-2) and hydrate formation (2-3); (b) Second injection stage (3-4) and hydrate formation (4-5); (c) Third injection stage (5-6) and hydrate formation (6-7); (d) Depressurization from reactor pressure to production pressure (7-8) and hydrate dissociation at constant pressure (8-9).

Similarly, the cycle of pressure fluctuation continues till hydrate is completely dissociated at constant dissociation pressure of 2.7 MPa. Cycles of pressure fluctuations seen in figure 6 have higher frequency during the earlier period of hydrate dissociation because of higher hydrate dissociation rate. However, the frequency drops as the dissociation rate becomes slower. Hydrate dissociation is also marked by a decrease in temperature because of its endothermic nature. Moreover, the sharp decrease in temperature marks a higher dissociation rate Zhou et al., 2009). However, temperature recovers itself after sometime as it gains heat from surroundings. Temperature close to the wall shows a quick rise as compared to the internal temperature sensors because of higher cooling at the wall.

Figure 7 shows the instantaneous gas flow rates. As the depressurization pressure is set, the initial free gas inside the reactor is released by the back-pressure regulator which is highlighted in fig. 7 and can be depicted by a sharp rise in flow rate followed by the actual dissociation of hydrates triggered due to the deviation from the equilibrium condition. The actual dissociation of gas is a very slow process and takes almost 35hrs to complete. Gas hydrate dissociation process generates water as per Eq. (1). Significant amount of water has been collected during hydrate dissociation, i.e., 207 gm.

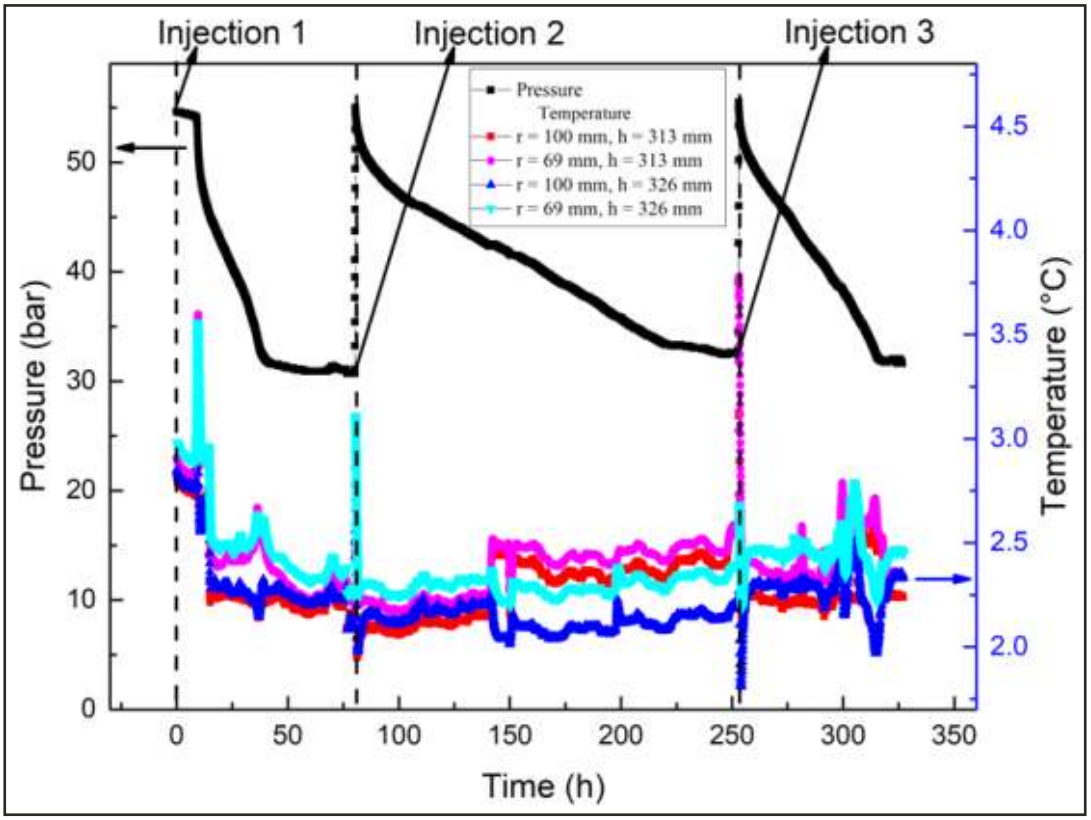

Fig. 6: Pressure and temperature variation at different radial (r) and axial locations (h) during hydrate dissociation by depressurization.

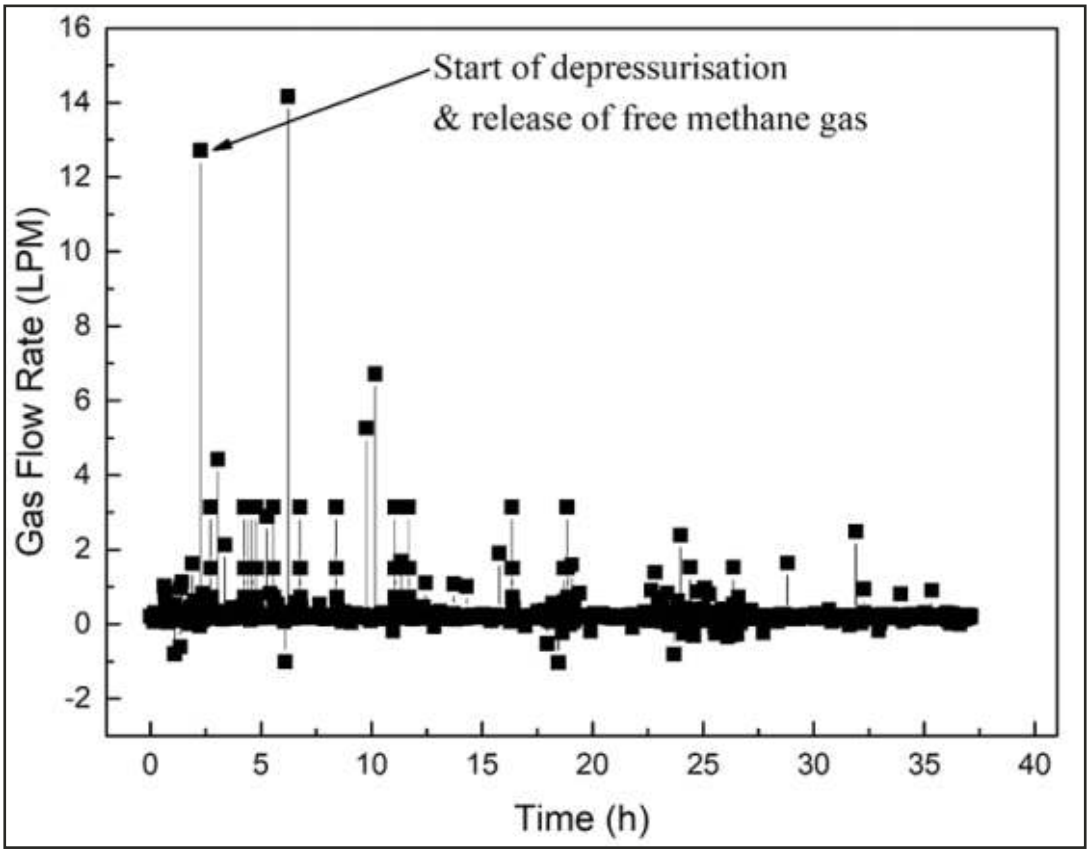

Fig. 7: Instantaneous methane gas flow rate during the hydrate dissociation.

CONCLUSIONS

Methane hydrate formation and dissociation have been carried out in a 25 L reactor. The formation process uses a multi step injection process to produce desired hydrate saturation and circumvent the large pressure requirement. Multi-point temperature measurements were carried out to investigate the temperature distribution inside the porous media. Important observations from the present study can be summarized as follows:

- Predetermined saturations level can be achieved in hydrate-bearing porous media using a multi-step gas injection method that eliminates the requirement for higher pressure inside the reaction chamber.
- Both the fugacity difference between equilibrium pressure and actual pressure and the transport within the hydrate-bearing sediments affect the hydrate formation rate.
- Hydrate dissociation is associated with periodic variation of pressure due to cycle of pressure build-up and release during depressurization of hydrate-bearing porous media.

ACKNOWLEDGMENTS

The authors gratefully acknowledge the valuable support and funding from Oil and Natural Gas Corporation, Govt. of India. The view expressed in this paper are those of the authors only.

References

Anderson, F.E., Prausnitz, J.M. (1986) Inhibition of gas hydrates by methanol. AIChE J. 32, 1321–1333. https://doi.org/10.1002/aic.690320810

Bishnoi, P.R., Dholabhai, P.D. (1993) Experimental study on propane hydrate equilibrium conditions in aqueous electrolyte solutions. Fluid Phase Equilib. 83, 455–462. https://doi.org/10.1007/s10870-010-9900-x

Chong, Z.R., Moh, J.W.R., Yin, Z., Zhao, J., Linga, P. (2018) Effect of vertical wellbore incorporation on energy recovery from aqueous rich hydrate sediments. Appl. Energy 229, 637–647. https://doi.org/10.1016/j.apenergy.2018.08.020.

Chong, Z.R., Yang, M., Khoo, B.C., Linga, P. (2016) Size Effect of Porous Media on Methane Hydrate Formation and Dissociation in an Excess Gas Environment. Ind. Eng. Chem. Res. 55, 7981–7991. https://doi.org/10.1021/acs.iecr.5b03908

Chong, Z.R., Yin, Z., Tan, J.H.C., Linga, P. (2017) Experimental investigations on energy recovery from water-saturated hydrate bearing sediments via depressurization approach. Appl. Energy 204, 1513–1525. https://doi.org/10.1016/j.apenergy.2017.04.031.

Davy, H. (1811) The Bakerian Lecture. On Some of the Combinations of Oxymuriatic Gas and Oxygen, and on the Chemical Relations of These Principles, to Inflammable Bodies. Proc. R. Soc. London 1, 385–388. https://doi.org/10.1098/rspl.1800.0216

Demirbas, A. (2010) Methane hydrates as potential energy resource: Part 1-Importance, resource and recovery facilities. Energy Convers. Manag. 51, 1547–1561. https://doi.org/DOI 10.1016/j.enconman. 2010.02.013

Haacke, R.R., Westbrook, G.K., Hyndman, R.D. (2007) Gas hydrate, fluid flow and free gas: Formation of the bottom-simulating reflector. Earth Planet. Sci. Lett. 261, 407–420. https://doi.org/10.1016/j.epsl.2007.07.008

Hammerschmidt, E.G., Natural, T., Company, G. (1934) Formation of Gas Hydrates in Natural Gas Transmission Lines 1934. https://doi.org/10.1021/ie50296a010

Indian Standard, IS: 2386 (Part III) "Methods of test for aggregates for concrete. Part III, Specific gravity, Density, Voids, Absorption and bulking", UDC 691:531:75 (1963) https://archive.org/details/gov.in.is.2386.3.1963/page/n3

Kvenvolden, K.A. (1988) Methane hydrate - A major reservoir of carbon in the shallow geosphere? Chem. Geol. https://doi.org/10.1016/0009-2541(88)90104-0

Li, X. Sen, Wan, L.H., Li, G., Li, Q.P., Chen, Z.Y., Yan, K.F. (2008) Experimental investigation into the production behavior of methane hydrate in porous sediment with hot brine stimulation. Ind. Eng. Chem. Res. 47, 9696–9702. https://doi.org/10.1021/ie8009582

Li, X. Sen, Yang, B., Li, G., Li, B., Zhang, Y., Chen, Z.Y. (2012) Experimental study on gas production from methane hydrate in porous media by huff and puff method in pilot-scale hydrate simulator. Fuel 94, 486–494. https://doi.org/10.1016/j.fuel.2011.11.011

Li, X., Wan, L., Li, G., Li, Q., Chen, Z., Yan, K. (2008) Experimental Investigation into the Production Behaviour of Methane Hydrate in 9696–9702.

Liu, B., Yuan, Q., Su, K.H., Yang, X., Wu, B.C., Sun, C.Y., Chen, G.J. (2012a) Experimental simulation of the exploitation of natural gas hydrate. Energies 5, 466–493. https://doi.org/10.3390/en5020466

Liu, B., Yuan, Q., Su, K.H., Yang, X., Wu, B.C., Sun, C.Y., Chen, G.J. (2012b) Experimental simulation of the exploitation of natural gas hydrate. Energies 5, 466–493. https://doi.org/10.3390/en5020466

Makogon, Y. F. (1965) Hydrate formation in the gas-bearing beds under permafrost conditions. Gazovaia Promyshlennost, 5, 14-15.

Mohammadi, A.H., Afzal, W., Richon, D. (2008) Gas hydrates of methane, ethane, propane, and carbon dioxide in the presence of single NaCl, KCl, and CaCl2 aqueous solutions: Experimental measurements and predictions of dissociation conditions. J. Chem. Thermodyn. 40, 1693–1697. https://doi.org/10.1016/j.jct.2008.06.015

Pitzer, K.S. (1955) The Volumetric and Thermodynamic Properties of Fluids. I. Theoretical Basis and Virial Coefficients. J. Am. Chem. Soc. 77, 3427–3433. https://doi.org/10.1021/ja01618a001

Priest, J.A., Rees, E.V.L., Clayton, C.R.I. (2009) Influence of gas hydrate morphology on the seismic velocities of sands. J. Geophys. Res. Solid Earth 114, 1–13. https://doi.org/10.1029/2009JB006284.

Reid, R.C., Prausnitz, J.M., Poling, B.E. (1987) The properties of gases & liquids, Experimental Thermal and Fluid Science. https://doi.org/10.1016/0894-1777(88)90021-0

Rong, C.Z. (2017) Methane Hydrate Formation and Dissociation in Porous Media (Ph.D. thesis, National University of Singapore). Retrieved from https://scholarbank.nus.edu.sg/handle/10635/3/browse?type=author&order=ASC&rpp=20&value=CHONG+ZHENG+RONG

Samimi, A. (2012) Preventing Hydrate Formation in Gas Transporting Pipe Lines with Synthetic Inhibitors. Int. J. Sci. Investig. Fr. 1, 48–50.

Sander, R. (2015) Compilation of Henry's law constants (version 4.0) for water as solvent 4399–4981. https://doi.org/10.5194/acp-15-4399-2015

Spangenberg, E., Kulenkampff, J., Naumann, R., Erzinger, J. (2005) Pore space hydrate formation in a glass bead sample from methane dissolved in water. Geophys. Res. Lett. 32, 1–4. https://doi.org/10.1029/2005GL024107

Spangenberg, E., Priegnitz, M., Heeschen, K., Schicks, J.M. (2015) Are laboratory-formed hydrate-bearing systems analogous to those in nature? J. Chem. Eng. Data 60, 258–268. https://doi.org/10.1021/je5005609

Stoll, R.D. (1979) Physical Properties of Sediments Containing Gas Hydrates. J. Geophys. Res. 84, 1629–1634.

Tang, L.-G., Xiao, R., Li, G., Feng, Z.-P., Li, X.-S., Fan, S.-S. (2006) Experimental investigation of production behavior of gas hydrate under thermal stimulation. Guocheng Gongcheng Xuebao/The Chinese J. Process Eng. 6, 2402–2407.

Tang, L.G., Li, X. Sen, Feng, Z.P., Li, G., Fan, S.S. (2007) Control mechanisms for gas hydrate production by depressurization in different scale hydrate reservoirs. Energy and Fuels 21, 227–233. https://doi.org/10.1021/ef0601869

Tupsakhare, S.S., Kattekola, S., Castaldi, M.J. (2017) An Application of the Results from the Large-Scale Thermal Stimulation Method of Methane Hydrate Dissociation to the Field Tests. Ind. Eng. Chem. Res. 56, 4588–4599. https://doi.org/10.1021/acs.iecr.7b00553.

Wang, Y., Li, X. Sen, Xu, W.Y., Li, Q.P., Zhang, Y., Li, G., Huang, N.S., Feng, J.C. (2013) Experimental investigation into factors influencing methane hydrate formation and a novel method for hydrate formation in porous media. Energy and Fuels 27, 3751–3757. https://doi.org/10.1021/ef400720h

Zhou, Y., Castaldi, M.J., Yegulalp, T.M. (2009) Experimental investigation of methane gas production from methane hydrate. Ind. Eng. Chem. Res. 48, 3142–3149. https://doi.org/10.1021/ie801004z

Nomenclature

C_a Concentration of methane in the aqueous phase (moles/L)

C_H Molar density of hydrate (moles/L)

C_w Molar density of water (moles/L)

f_t Fraction of initial moles utilized for hydrate formation at a given instant

$f_{t,i}$ Fraction of initial moles utilized for hydrate formation in i^{th} injection

M_h Molecular mass of hydrate (g)

M_w Molecular mass of water (g)

N Hydration number

n_H Moles of hydrate formed

n_{mt} Moles of gas required to achieve targeted hydrate saturation

$n_{m,a}$ Moles of methane in the aqueous form

$n_{m,g}$ Moles of methane in gaseous form

$n_{m,h}$ Moles of methane in hydrate form

n_m Moles of methane injected in the first injection

n_w Moles of water required to achieve targeted hydrate saturation

$n_{w,a}$ Moles of water present in the aqueous form

$n_{w,h}$ Moles of water converted into hydrate form

P Gas Pressure (bar)

P Partial pressure of that species in the gas phase under equilibrium conditions (bar)

R Real gas constant (KJ/Kg K)

S_g Gas saturation in hydrate form

S_h Hydrate Saturation

S_w Water Saturation

T Temperature (°C)

V_g Volume occupied by methane gas in the gaseous phase (L)

V_h Volume of the hydrate formed (L)

V_{pore} Pore volume of the sand medium (L)

V_w Volume of water injected (L)

υ_g Specific gas consumption (m^3/Kg)

ρ_h Density of hydrate formed (Kg/m^3)

ρ_w Density of water (Kg/m^3)

H'' Henry's law solubility constant at T = 298.5 K (mol/m^3Pa)

H Henry's law solubility constant (mol/m^3Pa)

Z Gas compressibility factor

Greek symbols

ρ Density (Kg/L)

ω Acentric factor

Subscripts

a Aqueous phase

c Critical temperature

g Gas phase

h Hydrate

i Gas injection stage

m Methane gas

t Time

w Water